

Supporting information

Conical-Shaped Titania Nanotubes for Optimized Light  
Management in DSSCs Reach Back-side Illumination Efficiencies  
> 8%

*Seulgi So,<sup>||†Δ</sup> Arian Kriesch,<sup>||‡Δ</sup> Ulf Peschel<sup>‡§Δ</sup> and Patrik Schmuki\*<sup>†Δ</sup>*

*<sup>†</sup>Department of Materials Science and Engineering, WW4-LKO, Friedrich-Alexander-University Erlangen-Nuremberg (FAU), Martensstrasse 7, 91058 Erlangen, Germany*

*<sup>‡</sup>Institute of Optics, Information and Photonics and Erlangen Graduate School in Advanced Optical Technologies (SAOT), Friedrich-Alexander-University Erlangen-Nuremberg (FAU), 91058 Erlangen, Germany*

*<sup>§</sup>Institute of Solid State Theory and Optics, Friedrich-Schiller-University Jena, 07743 Jena, Germany*

*<sup>Δ</sup>Cluster of Excellence Engineering of Advanced Materials (EAM), Friedrich-Alexander-University Erlangen-Nuremberg (FAU), 91058 Erlangen, Germany*

## Experimental Section

To grow TiO<sub>2</sub> nanotube layers we used titanium foils (0.125 mm thick, 99.6+% purity, Advent, England) that were degreased by sonication in acetone, ethanol and isopropanol, rinsed with deionized water, and then dried with a nitrogen jet. For cylinder shape nanotube layer (Cy), anodization was carried out with a high-voltage potentiostat (Jaissle IMP 88 PC) at 120 V in a two-electrode configuration with a counter electrode made of platinum gauze, using an electrolyte composition of 1.5 M lactic acid (LA, DL-Lactic acid, ~90 %, Fluka), 0.1 M ammonium fluoride (NH<sub>4</sub>F) and 5 wt % deionized H<sub>2</sub>O in ethylene glycol (99 vol %) held at a temperature of 60 °C (HAAKE F3 Thermostat) for 1 min.<sup>1</sup> The formed anodic nanotube layers from this first anodization were removed by ultra-sonication. In a second anodization, we used the same experimental conditions. For conical shaped nanotube layers (Con), anodization was carried out at 60V in two-electrode configuration using an electrolyte composed of 0.2 M ammonium fluoride (NH<sub>4</sub>F), 50 vol % lactic acid (LA, dl-lactic acid, ~90 %, Fluka), and 50 vol% tri-ethyleneglycol (99 vol %) held at 50 °C with a string using a hotplate for 20h.

In order to convert the TiO<sub>2</sub> nanotubes to anatase, the samples were annealed at 450 °C in air with a heating and cooling rate of 30 °C/min during 1 h using a Rapid Thermal Annealer.

For morphological characterization, a field-emission scanning electron microscope (FE-SEM, Hitachi SEM FE 4800) was used. The thickness of the nanotubes was measured from SEM cross-sections. Further morphological and structural characterization of the TiO<sub>2</sub> nanostructures was carried out with a TEM (Philips CM30 TEM/STEM). X-ray diffraction analysis (XRD, X'pert Philips PMD with a Panalytical X'celerator detector) with graphite monochromatized CuK $\alpha$  radiation (Wavelength 1.54056 Å) was used for determining the crystal structure of the samples (all samples used here were fully converted to anatase).

For diffuse and specular reflectance measurements with a Lambda 950 UV/Vis/NIR spectrophotometer with a 150 mm integrating sphere (Perkin Elmer), the TiO<sub>2</sub> nanotube samples were placed at the back of the sphere.

**DSSCs:** For dye-sensitization, Ru-based dye (cis-bis (isothiocyanato) bis (2,2- bipyridyl 4,4-dicarboxylato) ruthenium(II) bis-tetrabutylammonium) (D719, Everlight, Taiwan, same as usually used "N719 dye<sup>2</sup>") was used. Samples were dye-sensitized by immersing them for 1 day in a 300 mM solution of the Ru-based dye in a mixture of acetonitrile and tert-butyl alcohol (volume ratio: 1:1). After dye-sensitization, the

samples were rinsed with acetonitrile to remove non-chemisorbed dye. To evaluate the photovoltaic performance, the sensitized nanotubes were sandwiched together with a Pt coated fluorine-doped glass counter electrode (TCO22-15, Solaronix) using a polymer adhesive spacer (Surlyn, Dupont). Electrolyte (0.60 M BMIM-I, 0.03 M I<sub>2</sub>, 0.10 M GTC in acetonitril/ valeronitril (85:15 vol.)/ SB-163, IoLiTec Inc, Germany) was introduced into the space between the sandwiched cells. Using back-side illumination, the current-voltage characteristics of the cells were measured under simulated AM 1.5 illumination provided by a solar simulator (300 W Xe with optical filter, Solarlight), applying an external bias to the cell and measuring the generated photocurrent with a Keithley model 2420 digital source meter. The active area was defined by the opening of a black shadow film-mask to be 0.2 cm<sup>2</sup>. Incident photon-to-current conversion efficiency (IPCE) measurements were performed with a 150 W Xe arc lamp (LOT-Oriel Instruments) with an Oriel Cornerstone 7400 1/8 m monochromator. The light intensity was measured with an optical power meter.

For TiCl<sub>4</sub> treatments<sup>2</sup> we used 0.1 M aqueous solutions of TiCl<sub>4</sub> prepared under ice-cooled conditions. The TiO<sub>2</sub> nanotube layers were then treated at 70 °C for 30 min. Afterwards, the samples were washed with DI water and rinsed with ethanol to remove any excess TiCl<sub>4</sub>, and finally dried in a nitrogen jet. After the treatment, TiO<sub>2</sub> nanotube samples were annealed again at 450 °C for 10 min to crystallize attached nanoparticles.

Dye desorption measurements of the dye sensitized TiO<sub>2</sub> layers were carried out by immersing the samples in 5 ml of 10 mM KOH for 30 min. The concentration of fully desorbed dye was measured spectroscopically (using a Lambda XLS UV/VIS spectrophotometer, PerkinElmer) at 520 nm and the calculated amount of dye absorption on the TiO<sub>2</sub> nanotube layer using the Beer–Lambert law.

**IMPS-IMVS:** Intensity modulated photovoltage and photocurrent spectroscopy (IMPS) measurements were carried out using modulated light (10 % modulation depth) from a high power green LED ( $\lambda = 530$  nm) and UV ( $\lambda = 325$  nm). The modulation frequency was controlled by a frequency response analyzer (FRA, Zahner IM6) and the photocurrent or photovoltage of the cell was measured using an electrochemical interface (Zahner IM6), and fed back into FRA for analysis. The light incident intensity on the cell was measured using a calibrated Si photodiode.

**Simulation:**

**Numeric simulations:** The investigated system was simulated with the finite difference time domain (FDTD) method, applying the commercial FDTD solver package FDTD solutions by Lumerical Solutions Inc. based on Maxwell's equations. The system was excited with a linearly polarized plane wave, perpendicularly incident to the sample from top (compare Figure 3a, b) with an excitation spectrum that covered  $\lambda_0 = 400 \text{ nm} - 1 \mu\text{m}$ . The simulation domain was defined as a single unit cell of a rectangular lattice of the cylinders, respectively cones with geometry parameters determined from SEM analysis of the experimental samples with periodic boundary conditions in the in-plane dimensions ( $x, y$ ) and perfectly matched layers (PML) constraining the simulation domain in the  $z$  dimension. After a time-to-frequency Fourier transformation of the calculated electromagnetic fields, the reflectivity and absorption in the system were carefully calculated with power integration methods and particularly full spectral absorption profiles were extracted to give the full vertical volume optical power absorption along the  $z$  domain. The spectral absorptions, as calculated for a flat spectrum, were normalized to represent the correct absorption of an incident standard solar spectrum according to the AM 1.5, ASTM G173-03(2012) atmospheric global standard.<sup>3</sup> Due to the  $\text{TiO}_2$  band edge absorption, taking place below  $\lambda_0 \approx 400 \text{ nm}$ , the range for spectral absorption integration that is assumed to significantly contribute to the total photovoltaic efficiency, was chosen as  $\lambda_0 = 400 \text{ nm} - 1 \mu\text{m}$ . All presented spectral absorptions and spectrally integrated absorptions were globally normalized to the total integrated incident solar power within that range (Figure 3c and d).

**Material properties  $\text{TiO}_2$ :** The optical properties of  $\text{TiO}_2$  were modeled throughout  $\lambda_0 = 200 \text{ nm} - 1 \mu\text{m}$  for the anatase crystal configuration, according to experimental specifications. The experimental literature values<sup>4,5</sup> in accordance with Tang et al.<sup>6</sup> show an absorption band edge around  $\lambda_0 \approx 400 \text{ nm}$ , below which the optical absorption in the  $\text{TiO}_2$  rapidly increases. This material was applied to the bulk  $\text{TiO}_2$  that forms the cones, respectively the cylinders and for the subwavelength  $\text{TiO}_2$  nanocrystals.

**Material properties dye:** The optical properties of the standard dye with ruthenium complex  $[\text{Ru}(\text{dcbpyH}_2)_2(\text{NCS})_2]$  were modeled for  $\lambda_0 = 200 \text{ nm} - 1 \mu\text{m}$  following experimental absorbance spectra from Nazeeruddin et al.<sup>7</sup> by tuning a double-Lorentzian resonance model for the spectral position and widths of the two absorption peaks at  $\lambda_{0,1} = 380 \text{ nm} \pm 10 \text{ nm}$  and  $\lambda_{0,2} = 515 \text{ nm} \pm 10 \text{ nm}$ .

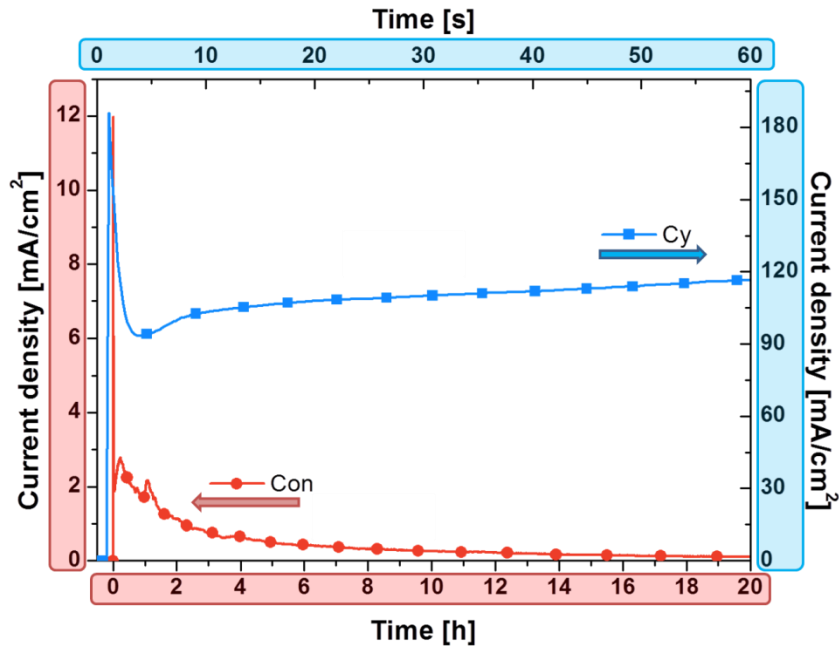
**Material model with Maxwell-Garnett-Theory:** The composite material consisting of 50% volume fraction of  $\text{TiO}_2$  nanocrystals and of 50% volume fraction of dye was modelled following Maxwell-Garnett theory (MGT).<sup>8,9</sup> To match the experimental density of the dye in the composite material, the imaginary part of the permittivity was varied and the real part was recalculated to match the double Lorentzian

dispersion accordingly, while the full FDTD simulations were iteratively executed and the absorption and reflection results were compared with experimental values.

Some simulation parameters, including the concentration of the dye as the active absorbing substance, were only known within certain ranges. Therefore, we conducted extensive variations in particular of the density of the dye within the Maxwell-Garnett medium to find the most reasonable configuration. A further increase of the optical density of the dye reduced the substrate absorption, but always leads to a shift of the vertical power absorption balance to the top layers. In that case the enhancement by the cones over the cylinders would probably vanish and the differential power absorption (Figure 3c) both approaches an exponential power decay characteristic.

**Figure S1**

Current density transients for cylinder (Cy) and conical (Con) shaped nanotubes in 1.5 M lactic acid, 0.1 M  $\text{NH}_4\text{F}$  and 5 wt % deionized  $\text{H}_2\text{O}$  in ethylene glycol electrolyte at 120 V (Cy) and in 0.2 M  $\text{NH}_4\text{F}$ , 50 vol % lactic acid, and 50 vol % tri-ethyleneglycol electrolyte at 60 V (Con).



As evident from the  $I-t$  curve the conical shape tubes grow much slower with key difference being the electrolyte conductivity ( $198 \mu\text{S}/\text{cm}$  for Con-electrolyte and  $440 \mu\text{S}/\text{cm}$  for Cy-electrolyte). In order to grow  $13 \mu\text{m}$  cylinder tubes in the Cy-electrolyte it takes 1min (i.e. virtually no change in anodizing condition occurs). In order to grow  $13 \mu\text{m}$  conical tubes it takes 20h. In this case the local changes in conductivity by reaction products lead to a permanent enhancement of the effective anodic voltage, and thus to an increase in diameter over time.

## S2-TiCl<sub>4</sub> decoration

In order to construct efficient solar cells from such large diameter tubes (cylinder or conical), the layers were decorated with TiO<sub>2</sub> nanoparticles by a TiCl<sub>4</sub> treatment<sup>2</sup> to increase the overall surface area (i.e. this increases the dye absorption per unit solar cell volume). The TiCl<sub>4</sub> treatment was carried out as described in the experimental section. In each TiO<sub>2</sub> deposition cycle the outer and inner decoration thickness increases by approx. 15 nm. Crystallites typically have a size of 3 nm, and after annealing form a rigidly attached nanoparticle coating on the tube wall. For both tube types we repeated the TiCl<sub>4</sub> step until a maximum solar cell efficiency was reached (see following pages). This occurred for cylindrical tubes after 2 cycles and for conical tubes after 5 cycles (see Figure S3). Nevertheless, dye loading measurements show that in both cases almost the same amount of dye (and thus TiO<sub>2</sub> nanoparticles were deposited) to reach a maximum. Moreover, in Figure S2a, b, Con sample after 5 cycles of 0.1 M TiCl<sub>4</sub> treatment, we see that the cones are well decorated on the top and are still open. Attempts to decorate more than 7 cycles leads to partial blockage of the tubes by TiO<sub>2</sub> nanoparticles (Figure S2a). In Cy tube case only 2 cycles of TiCl<sub>4</sub> treatments could be performed without any blockage of the tubes (Figure 2c, d), and 3 cycles start to block tubes (Figure S2b). Hence, Con sample with 5 cycles of nanoparticle decoration and Cy sample with 2 cycles of nanoparticle decoration are best conditions without any blockage (and have a very similar loading of dye).

**Figure S2(a)**

Top SEM images of Con nanotube samples for different 0.1M  $\text{TiCl}_4$  decoration times. (T1 = T(1time), T2=T(2times), etc.)

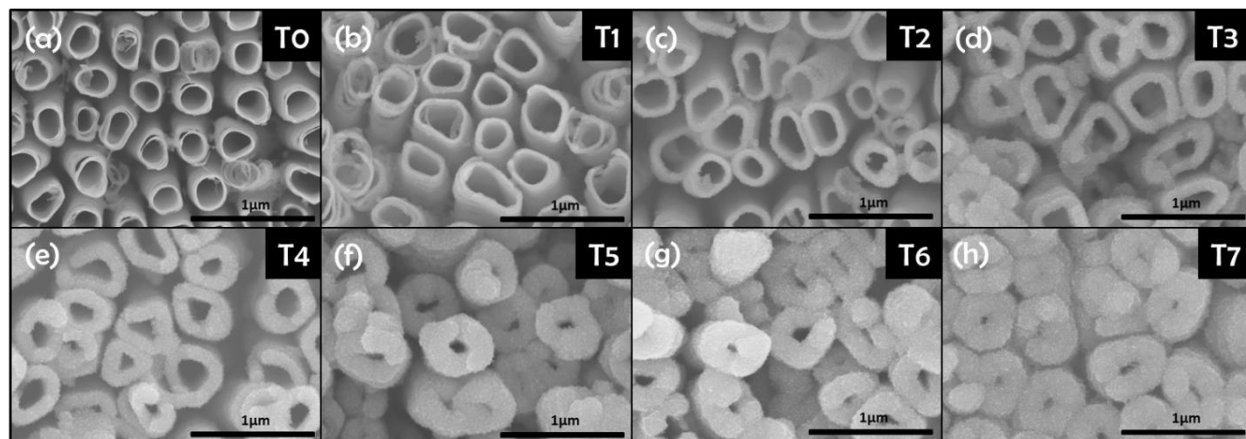


**Figure S2(b)**

Top SEM images of Cy nanotube samples for different 0.1M  $\text{TiCl}_4$  decoration times. (T1 = T(1time), T2=T(2times), etc.)

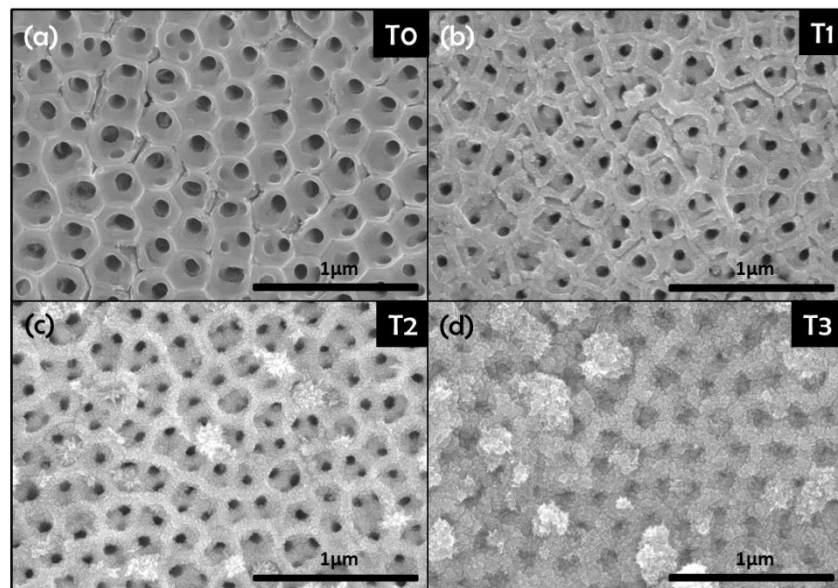
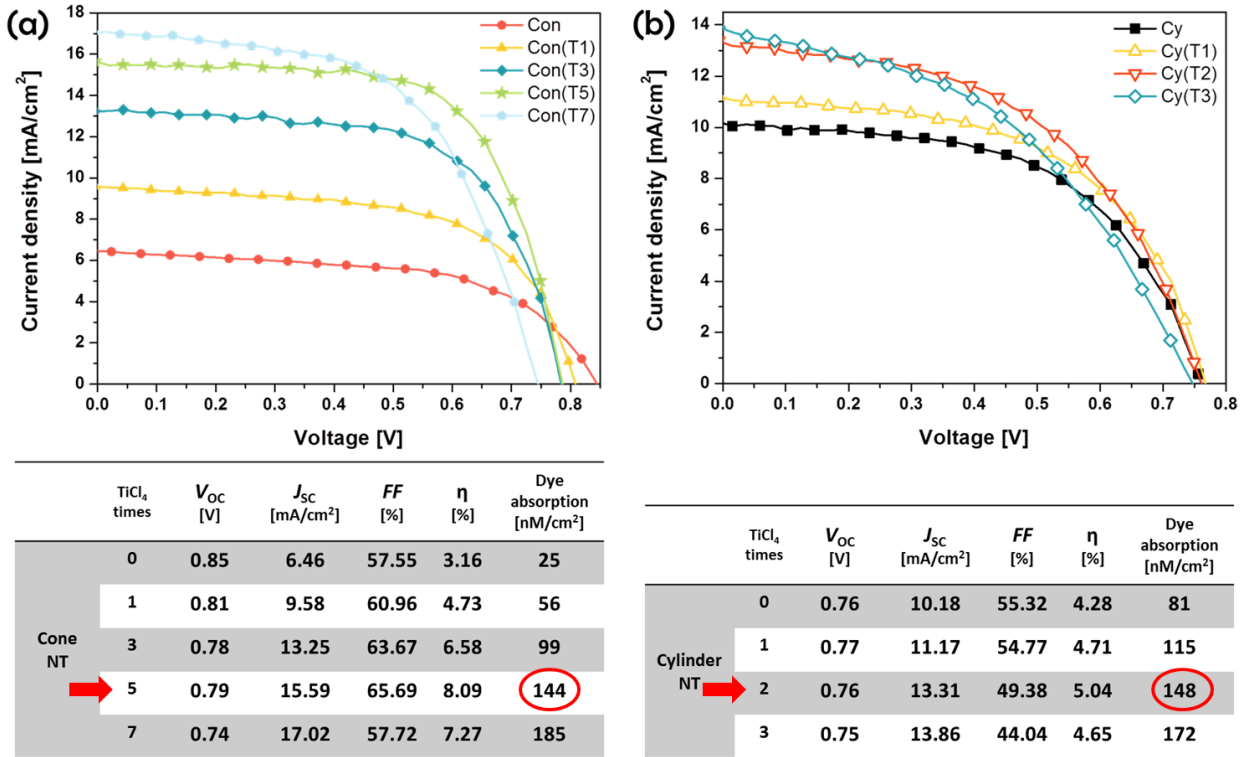


**Figure S3**

I–V characteristics for DSSCs fabricated using (a) conical and (b) cylinder nanotube samples with  $\text{TiCl}_4$  decoration using 13  $\mu\text{m}$  thickness tube layers. ( $J_{sc}$  = short-circuit current,  $V_{oc}$  = open-circuit voltage,  $FF$ = fill factor,  $\eta$  =efficiency)



As a result we can get the highest efficiency after 5 cycles of  $\text{TiCl}_4$  decoration on Con with an overall efficiency of 8.05 % with good fill factor for illumination with 1.5 solar simulators at  $100 \text{ mW}/\text{cm}^2$ . Higher particle loading, using 7 cycles of  $\text{TiCl}_4$  decoration, still leads to an increase in  $J_{sc}$  and dye adsorption, but fill factor ( $FF$ ) is considerably decreased, which as a consequence decreases conversion results efficiency (Figure S3a).

In S3b, we can compare also  $\text{TiCl}_4$  decoration properties with Cy tubes. We can observe with increasing number of  $\text{TiCl}_4$  treatments, that  $J_{sc}$  and the dye absorbance also increase - nevertheless a 2 times  $\text{TiCl}_4$  treatment leads to the best solar cell efficiency of 5.04 %. After that point the results start to decrease (Figure S2b).

**Figure S4**

(a) Electron transfer time ( $\tau_c$ ) and (b) recombination time ( $\tau_r$ ) constants from IMPS and IMVS measurements for conical samples with  $\text{TiCl}_4$  decoration.

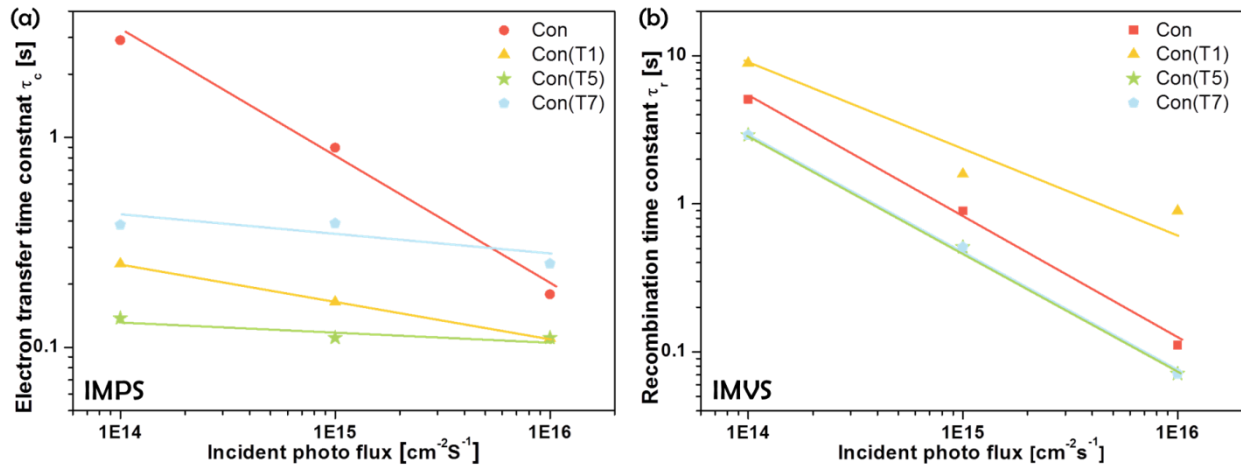


**Figure S5**

(a) Electron transfer time ( $\tau_c$ ) and (b) recombination time ( $\tau_r$ ) constants from IMPS and IMVS measurements for cylinder samples with  $\text{TiCl}_4$  decoration.

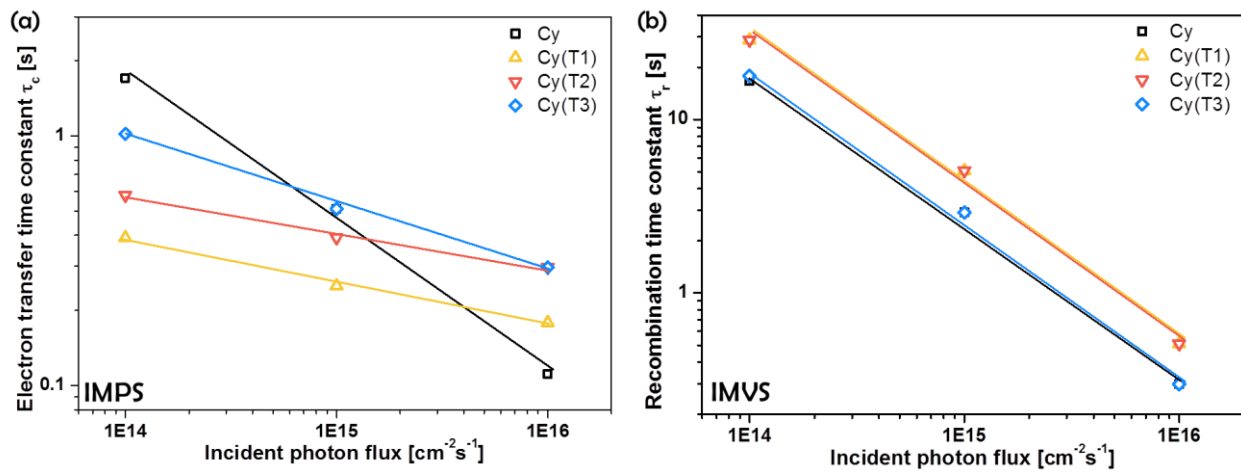


**Figure S6**

(a) Real and imaginary part of the relative permittivity of the  $\text{TiO}_2$  in the spectral range of the simulation. (b) Real and imaginary part of the relative permittivity of the dye material. (c) Relative permittivity calculated from Maxwell-Garnett-Theory with 50 % density of materials as shown in (a) and (b).

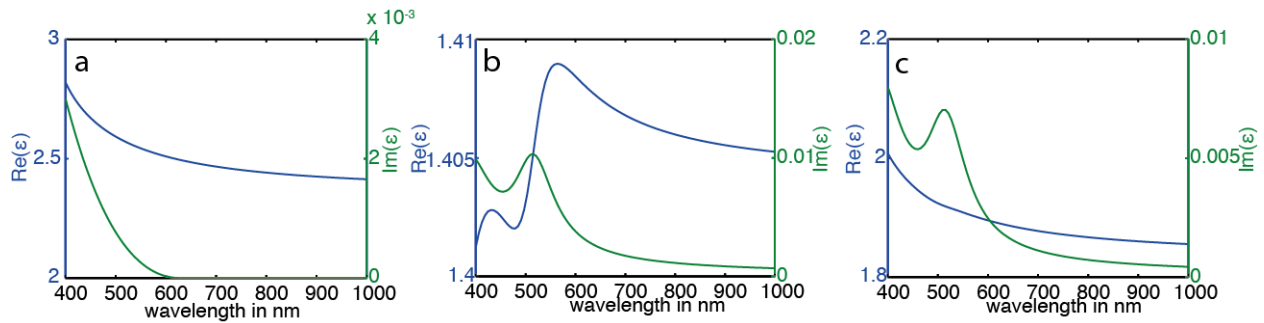
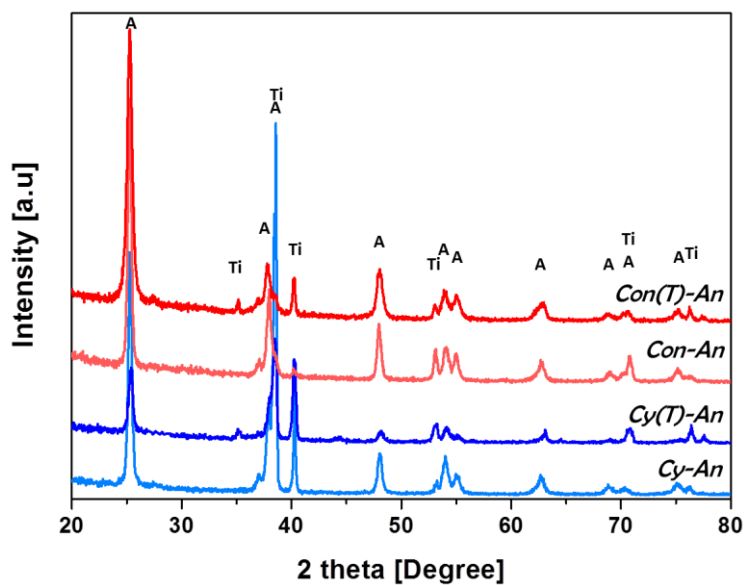


**Figure S7**

XRD spectra taken of conical and cylindrical samples with and without  $\text{TiCl}_4$  treatment samples after annealed at 450 °C. (Ti=titanium, A=anatase)



## Reference

1. S. So, K. Lee and P. Schmuki, *J. Am. Chem. Soc.*, 2012, **134**, 11316-11318.
2. M. K. Nazeeruddin, A. Kay, I. Rodicio, R. Humphry-Baker, E. Müller, P. Liska, N. Vlachopoulos and M. Grätzel, *J. Am. Chem. Soc.*, 1993, **115**, 6382-6390.
3. ASTM G173-03(2012), Standard Tables for Reference Solar Spectral Irradiances: Direct Normal and Hemispherical on 37° Tilted Surface, *ASTM International*, West Conshohocken, PA, **2012**, [www.astm.org](http://www.astm.org)
4. G. Liu, C. Sun, H. G. Yang, S. C. Smith, L. Wang, G. Q. Lu and H. M. Cheng, *Chem. Commun.*, 2010, **46**, 755-757.
5. J. R. Devore, *J. Opt. Soc. Am.*, 1951, **41**, 416.
6. H. Tang, K. Prasad, R. Sanjines, P. E. Schmid and F. Levy, *J. Appl. Phys.*, 1994, **75**, 2042-2047.
7. M. K. Nazeeruddin, S. M. Zakeeruddin, R. Humphry-Baker, M. Jirousek, P. Liska, N. Vlachopoulos, V. Shklover, C. H. Fischer and M. Grätzel, *Inorg. Chem.*, 1999, **38**, 6298.
8. J. C. M. Garnett, *Phil. Trans. R. Soc. A*, 1904, **203**, 385-420.
9. A. Garahan, L. Pilon, J. Yin and I. Saxena, *J. Appl. Phys.*, 2007, **101**.